

**Measurements of baryon pair decays of  $\chi_{cJ}$  mesons**

M. Ablikim,<sup>1</sup> M. N. Achasov,<sup>6</sup> O. Albayrak,<sup>3</sup> D. J. Ambrose,<sup>39</sup> F. F. An,<sup>1</sup> Q. An,<sup>40</sup> J. Z. Bai,<sup>1</sup> Y. Ban,<sup>26</sup> J. Becker,<sup>2</sup> J. V. Bennett,<sup>16</sup> M. Bertani,<sup>17a</sup> J. M. Bian,<sup>38</sup> E. Boger,<sup>19,\*</sup> O. Bondarenko,<sup>20</sup> I. Boyko,<sup>19</sup> R. A. Briere,<sup>3</sup> V. Bytev,<sup>19</sup> X. Cai,<sup>1</sup> O. Cakir,<sup>34a</sup> A. Calcaterra,<sup>17a</sup> G. F. Cao,<sup>1</sup> S. A. Cetin,<sup>34b</sup> J. F. Chang,<sup>1</sup> G. Chelkov,<sup>19,\*</sup> G. Chen,<sup>1</sup> H. S. Chen,<sup>1</sup> J. C. Chen,<sup>1</sup> M. L. Chen,<sup>1</sup> S. J. Chen,<sup>24</sup> X. Chen,<sup>26</sup> Y. B. Chen,<sup>1</sup> H. P. Cheng,<sup>14</sup> Y. P. Chu,<sup>1</sup> D. Cronin-Hennessy,<sup>38</sup> H. L. Dai,<sup>1</sup> J. P. Dai,<sup>1</sup> D. Dedovich,<sup>19</sup> Z. Y. Deng,<sup>1</sup> A. Denig,<sup>18</sup> I. Denysenko,<sup>19,†</sup> M. Destefanis,<sup>43a,43b</sup> W. M. Ding,<sup>28</sup> Y. Ding,<sup>22</sup> L. Y. Dong,<sup>1</sup> M. Y. Dong,<sup>1</sup> S. X. Du,<sup>46</sup> J. Fang,<sup>1</sup> S. S. Fang,<sup>1</sup> L. Fava,<sup>43b,43c</sup> C. Q. Feng,<sup>40</sup> R. B. Ferroli,<sup>17a</sup> P. Friedel,<sup>2</sup> C. D. Fu,<sup>1</sup> Y. Gao,<sup>33</sup> C. Geng,<sup>40</sup> K. Goetzen,<sup>7</sup> W. X. Gong,<sup>1</sup> W. Gradl,<sup>18</sup> M. Greco,<sup>43a,43c</sup> M. H. Gu,<sup>1</sup> Y. T. Gu,<sup>9</sup> Y. H. Guan,<sup>36</sup> A. Q. Guo,<sup>25</sup> L. B. Guo,<sup>23</sup> T. Guo,<sup>23</sup> Y. P. Guo,<sup>25</sup> Y. L. Han,<sup>1</sup> F. A. Harris,<sup>37</sup> K. L. He,<sup>1</sup> M. He,<sup>1</sup> Z. Y. He,<sup>25</sup> T. Held,<sup>2</sup> Y. K. Heng,<sup>1</sup> Z. L. Hou,<sup>1</sup> C. Hu,<sup>23</sup> H. M. Hu,<sup>1</sup> J. F. Hu,<sup>35</sup> T. Hu,<sup>1</sup> G. M. Huang,<sup>4</sup> G. S. Huang,<sup>40</sup> J. S. Huang,<sup>12</sup> L. Huang,<sup>1</sup> X. T. Huang,<sup>28</sup> Y. Huang,<sup>24</sup> Y. P. Huang,<sup>1</sup> T. Hussain,<sup>42</sup> C. S. Ji,<sup>40</sup> Q. Ji,<sup>1</sup> Q. P. Ji,<sup>25</sup> X. B. Ji,<sup>1</sup> X. L. Ji,<sup>1</sup> L. L. Jiang,<sup>1</sup> X. S. Jiang,<sup>1</sup> J. B. Jiao,<sup>28</sup> Z. Jiao,<sup>14</sup> D. P. Jin,<sup>1</sup> S. Jin,<sup>1</sup> F. F. Jing,<sup>33</sup> N. Kalantar-Nayestanaki,<sup>20</sup> M. Kavatsyuk,<sup>20</sup> B. Kopf,<sup>2</sup> M. Kornicer,<sup>37</sup> W. Kuehn,<sup>35</sup> W. Lai,<sup>1</sup> J. S. Lange,<sup>35</sup> M. Leyhe,<sup>2</sup> C. H. Li,<sup>1</sup> Cheng Li,<sup>40</sup> Cui Li,<sup>40</sup> D. M. Li,<sup>46</sup> F. Li,<sup>1</sup> G. Li,<sup>1</sup> H. B. Li,<sup>1</sup> J. C. Li,<sup>1</sup> K. Li,<sup>10</sup> Lei Li,<sup>1</sup> Q. J. Li,<sup>1</sup> S. L. Li,<sup>1</sup> W. D. Li,<sup>1</sup> W. G. Li,<sup>1</sup> X. L. Li,<sup>28</sup> X. N. Li,<sup>1</sup> X. Q. Li,<sup>25</sup> X. R. Li,<sup>27</sup> Z. B. Li,<sup>32</sup> H. Liang,<sup>40</sup> Y. F. Liang,<sup>30</sup> Y. T. Liang,<sup>35</sup> G. R. Liao,<sup>33</sup> X. T. Liao,<sup>1</sup> D. Lin,<sup>11</sup> B. J. Liu,<sup>1</sup> C. L. Liu,<sup>3</sup> C. X. Liu,<sup>1</sup> F. H. Liu,<sup>29</sup> Fang Liu,<sup>1</sup> Feng Liu,<sup>4</sup> H. Liu,<sup>1</sup> H. B. Liu,<sup>9</sup> H. H. Liu,<sup>13</sup> H. M. Liu,<sup>1</sup> H. W. Liu,<sup>1</sup> J. P. Liu,<sup>44</sup> K. Liu,<sup>33</sup> K. Y. Liu,<sup>22</sup> Kai Liu,<sup>36</sup> P. L. Liu,<sup>28</sup> Q. Liu,<sup>36</sup> S. B. Liu,<sup>40</sup> X. Liu,<sup>21</sup> Y. B. Liu,<sup>25</sup> Z. A. Liu,<sup>1</sup> Zhiqiang Liu,<sup>1</sup> Zhiqing Liu,<sup>1</sup> H. Loehner,<sup>20</sup> G. R. Lu,<sup>12</sup> H. J. Lu,<sup>14</sup> J. G. Lu,<sup>1</sup> Q. W. Lu,<sup>29</sup> X. R. Lu,<sup>36</sup> Y. P. Lu,<sup>1</sup> C. L. Luo,<sup>23</sup> M. X. Luo,<sup>45</sup> T. Luo,<sup>37</sup> X. L. Luo,<sup>1</sup> M. Lv,<sup>1</sup> C. L. Ma,<sup>36</sup> F. C. Ma,<sup>22</sup> H. L. Ma,<sup>1</sup> Q. M. Ma,<sup>1</sup> S. Ma,<sup>1</sup> T. Ma,<sup>1</sup> X. Y. Ma,<sup>1</sup> F. E. Maas,<sup>11</sup> M. Maggiora,<sup>43a,43c</sup> Q. A. Malik,<sup>42</sup> Y. J. Mao,<sup>26</sup> Z. P. Mao,<sup>1</sup> J. G. Messchendorp,<sup>20</sup> J. Min,<sup>1</sup> T. J. Min,<sup>1</sup> R. E. Mitchell,<sup>16</sup> X. H. Mo,<sup>1</sup> C. Morales Morales,<sup>11</sup> N. Yu. Muchnoi,<sup>6</sup> H. Muramatsu,<sup>39</sup> Y. Nefedov,<sup>19</sup> C. Nicholson,<sup>36</sup> I. B. Nikolaev,<sup>6</sup> Z. Ning,<sup>1</sup> S. L. Olsen,<sup>27</sup> Q. Ouyang,<sup>1</sup> S. Pacetti,<sup>17b</sup> J. W. Park,<sup>27</sup> M. Pelizaeus,<sup>2</sup> H. P. Peng,<sup>40</sup> K. Peters,<sup>7</sup> J. L. Ping,<sup>23</sup> R. G. Ping,<sup>1</sup> R. Poling,<sup>38</sup> E. Prencipe,<sup>18</sup> M. Qi,<sup>24</sup> S. Qian,<sup>1</sup> C. F. Qiao,<sup>36</sup> L. Q. Qin,<sup>28</sup> X. S. Qin,<sup>1</sup> Y. Qin,<sup>26</sup> Z. H. Qin,<sup>1</sup> J. F. Qiu,<sup>1</sup> K. H. Rashid,<sup>42</sup> G. Rong,<sup>1</sup> X. D. Ruan,<sup>9</sup> A. Sarantsev,<sup>19,‡</sup> B. D. Schaefer,<sup>16</sup> M. Shao,<sup>40</sup> C. P. Shen,<sup>37,§</sup> X. Y. Shen,<sup>1</sup> H. Y. Sheng,<sup>1</sup> M. R. Shepherd,<sup>16</sup> X. Y. Song,<sup>1</sup> S. Spataro,<sup>43a,43c</sup> B. Spruck,<sup>35</sup> D. H. Sun,<sup>1</sup> G. X. Sun,<sup>1</sup> J. F. Sun,<sup>12</sup> S. S. Sun,<sup>1</sup> Y. J. Sun,<sup>40</sup> Y. Z. Sun,<sup>1</sup> Z. J. Sun,<sup>1</sup> Z. T. Sun,<sup>40</sup> C. J. Tang,<sup>30</sup> X. Tang,<sup>1</sup> I. Tapan,<sup>34c</sup> E. H. Thorndike,<sup>39</sup> D. Toth,<sup>38</sup> M. Ullrich,<sup>35</sup> G. S. Varner,<sup>37</sup> B. Q. Wang,<sup>26</sup> D. Wang,<sup>26</sup> D. Y. Wang,<sup>26</sup> K. Wang,<sup>1</sup> L. L. Wang,<sup>1</sup> L. S. Wang,<sup>1</sup> M. Wang,<sup>28</sup> P. Wang,<sup>1</sup> P. L. Wang,<sup>1</sup> Q. J. Wang,<sup>1</sup> S. G. Wang,<sup>26</sup> X. F. Wang,<sup>33</sup> X. L. Wang,<sup>40</sup> Y. F. Wang,<sup>1</sup> Z. Wang,<sup>1</sup> Z. G. Wang,<sup>1</sup> Z. Y. Wang,<sup>1</sup> D. H. Wei,<sup>8</sup> J. B. Wei,<sup>26</sup> P. Weidenkaff,<sup>18</sup> Q. G. Wen,<sup>40</sup> S. P. Wen,<sup>1</sup> M. Werner,<sup>35</sup> U. Wiedner,<sup>2</sup> L. H. Wu,<sup>1</sup> N. Wu,<sup>1</sup> S. X. Wu,<sup>40</sup> W. Wu,<sup>25</sup> Z. Wu,<sup>1</sup> L. G. Xia,<sup>33</sup> Z. J. Xiao,<sup>23</sup> Y. G. Xie,<sup>1</sup> Q. L. Xiu,<sup>1</sup> G. F. Xu,<sup>1</sup> G. M. Xu,<sup>26</sup> Q. J. Xu,<sup>10</sup> Q. N. Xu,<sup>36</sup> X. P. Xu,<sup>31</sup> Z. R. Xu,<sup>40</sup> F. Xue,<sup>4</sup> Z. Xue,<sup>1</sup> L. Yan,<sup>40</sup> W. B. Yan,<sup>40</sup> Y. H. Yan,<sup>15</sup> H. X. Yang,<sup>1</sup> Y. Yang,<sup>4</sup> Y. X. Yang,<sup>8</sup> H. Ye,<sup>1</sup> M. Ye,<sup>1</sup> M. H. Ye,<sup>5</sup> B. X. Yu,<sup>1</sup> C. X. Yu,<sup>25</sup> H. W. Yu,<sup>26</sup> J. S. Yu,<sup>21</sup> S. P. Yu,<sup>28</sup> C. Z. Yuan,<sup>1</sup> Y. Yuan,<sup>1</sup> A. A. Zafar,<sup>42</sup> A. Zallo,<sup>17a</sup> Y. Zeng,<sup>15</sup> B. X. Zhang,<sup>1</sup> B. Y. Zhang,<sup>1</sup> C. Zhang,<sup>24</sup> C. C. Zhang,<sup>1</sup> D. H. Zhang,<sup>1</sup> H. H. Zhang,<sup>32</sup> H. Y. Zhang,<sup>1</sup> J. Q. Zhang,<sup>1</sup> J. W. Zhang,<sup>1</sup> J. Y. Zhang,<sup>1</sup> J. Z. Zhang,<sup>1</sup> R. Zhang,<sup>36</sup> S. H. Zhang,<sup>1</sup> X. J. Zhang,<sup>1</sup> X. Y. Zhang,<sup>28</sup> Y. Zhang,<sup>1</sup> Y. H. Zhang,<sup>1</sup> Z. P. Zhang,<sup>40</sup> Z. Y. Zhang,<sup>44</sup> Zhenghao Zhang,<sup>4</sup> G. Zhao,<sup>1</sup> H. S. Zhao,<sup>1</sup> J. W. Zhao,<sup>1</sup> K. X. Zhao,<sup>23</sup> Lei Zhao,<sup>40</sup> Ling Zhao,<sup>1</sup> M. G. Zhao,<sup>25</sup> Q. Zhao,<sup>1</sup> Q. Z. Zhao,<sup>9</sup> S. J. Zhao,<sup>46</sup> T. C. Zhao,<sup>1</sup> Y. B. Zhao,<sup>1</sup> Z. G. Zhao,<sup>40</sup> A. Zhemchugov,<sup>19,\*</sup> B. Zheng,<sup>41</sup> J. P. Zheng,<sup>1</sup> Y. H. Zheng,<sup>36</sup> B. Zhong,<sup>23</sup> Z. Zhong,<sup>9</sup> L. Zhou,<sup>1</sup> X. K. Zhou,<sup>36</sup> X. R. Zhou,<sup>40</sup> C. Zhu,<sup>1</sup> K. Zhu,<sup>1</sup> K. J. Zhu,<sup>1</sup> S. H. Zhu,<sup>1</sup> X. L. Zhu,<sup>33</sup> Y. C. Zhu,<sup>40</sup> Y. M. Zhu,<sup>25</sup> Y. S. Zhu,<sup>1</sup> Z. A. Zhu,<sup>1</sup> J. Zhuang,<sup>1</sup> B. S. Zou,<sup>1</sup> and J. H. Zou<sup>1</sup>

(BESIII Collaboration)

<sup>1</sup>*Institute of High Energy Physics, Beijing 100049, People's Republic of China*<sup>2</sup>*Bochum Ruhr-University, D-44780 Bochum, Germany*<sup>3</sup>*Carnegie Mellon University, Pittsburgh, Pennsylvania 15213, USA*<sup>4</sup>*Central China Normal University, Wuhan 430079, People's Republic of China*<sup>5</sup>*China Center of Advanced Science and Technology, Beijing 100190, People's Republic of China*<sup>6</sup>*G.I. Budker Institute of Nuclear Physics SB RAS (BINP), Novosibirsk 630090, Russia*<sup>7</sup>*GSI Helmholtzcentre for Heavy Ion Research GmbH, D-64291 Darmstadt, Germany*<sup>8</sup>*Guangxi Normal University, Guilin 541004, People's Republic of China*<sup>9</sup>*GuangXi University, Nanning 530004, People's Republic of China*<sup>10</sup>*Hangzhou Normal University, Hangzhou 310036, People's Republic of China*<sup>11</sup>*Helmholtz Institute Mainz, Johann-Joachim-Becher-Weg 45, D-55099 Mainz, Germany*

- <sup>12</sup>Henan Normal University, Xinxiang 453007, People's Republic of China  
<sup>13</sup>Henan University of Science Technology, Luoyang 471003, People's Republic of China  
<sup>14</sup>Huangshan College, Huangshan 245000, People's Republic of China  
<sup>15</sup>Hunan University, Changsha 410082, People's Republic of China  
<sup>16</sup>Indiana University, Bloomington, Indiana 47405, USA  
<sup>17a</sup>INFN Laboratori Nazionali di Frascati, I-00044 Frascati, Italy  
<sup>17b</sup>INFN University of Perugia, I-06100 Perugia, Italy  
<sup>18</sup>Johannes Gutenberg University of Mainz, Johann-Joachim-Becher-Weg 45, D-55099 Mainz, Germany  
<sup>19</sup>Joint Institute for Nuclear Research, 141980 Dubna, Moscow region, Russia  
<sup>20</sup>KVI University of Groningen, NL-9747 AA Groningen, The Netherlands  
<sup>21</sup>Lanzhou University, Lanzhou 730000, People's Republic of China  
<sup>22</sup>Liaoning University, Shenyang 110036, People's Republic of China  
<sup>23</sup>Nanjing Normal University, Nanjing 210023, People's Republic of China  
<sup>24</sup>Nanjing University, Nanjing 210093, People's Republic of China  
<sup>25</sup>Nankai University, Tianjin 300071, People's Republic of China  
<sup>26</sup>Peking University, Beijing 100871, People's Republic of China  
<sup>27</sup>Seoul National University, Seoul, 151-747 Korea  
<sup>28</sup>Shandong University, Jinan 250100, People's Republic of China  
<sup>29</sup>Shanxi University, Taiyuan 030006, People's Republic of China  
<sup>30</sup>Sichuan University, Chengdu 610064, People's Republic of China  
<sup>31</sup>Soochow University, Suzhou 215006, People's Republic of China  
<sup>32</sup>Sun Yat-Sen University, Guangzhou 510275, People's Republic of China  
<sup>33</sup>Tsinghua University, Beijing 100084, People's Republic of China  
<sup>34a</sup>Ankara University, Dogol Caddesi, 06100 Tandogan, Ankara, Turkey  
<sup>34b</sup>Dogus University, 34722 Istanbul, Turkey  
<sup>34c</sup>Uludag University, 16059 Bursa, Turkey  
<sup>35</sup>Universitaet Giessen, D-35392 Giessen, Germany  
<sup>36</sup>University of Chinese Academy of Sciences, Beijing 100049, People's Republic of China  
<sup>37</sup>University of Hawaii, Honolulu, Hawaii 96822, USA  
<sup>38</sup>University of Minnesota, Minneapolis, Minnesota 55455, USA  
<sup>39</sup>University of Rochester, Rochester, New York 14627, USA  
<sup>40</sup>University of Science Technology of China, Hefei 230026, People's Republic of China  
<sup>41</sup>University of South China, Hengyang 421001, People's Republic of China  
<sup>42</sup>University of the Punjab, Lahore 54590, Pakistan  
<sup>43a</sup>University of Turin, I-10125 Turin, Italy  
<sup>43b</sup>University of Eastern Piedmont, I-15121 Alessandria, Italy  
<sup>43c</sup>INFN, I-10125 Turin, Italy  
<sup>44</sup>Wuhan University, Wuhan 430072, People's Republic of China  
<sup>45</sup>Zhejiang University, Hangzhou 310027, People's Republic of China  
<sup>46</sup>Zhengzhou University, Zhengzhou 450001, People's Republic of China

(Received 9 November 2012; published 15 February 2013; publisher error corrected 21 February 2013)

Using  $106 \times 10^6$   $\psi'$  decays collected with the BESIII detector at the BEPCII, three decays of  $\chi_{cJ}$  ( $J = 0, 1, 2$ ) with baryon pairs ( $\Lambda\bar{\Lambda}$ ,  $\Sigma^0\bar{\Sigma}^0$ ,  $\Sigma^+\bar{\Sigma}^-$ ) in the final state have been studied. The branching fractions are measured to be  $\mathcal{B}(\chi_{c0,1,2} \rightarrow \Lambda\bar{\Lambda}) = (33.3 \pm 2.0 \pm 2.6) \times 10^{-5}$ ,  $(12.2 \pm 1.1 \pm 1.1) \times 10^{-5}$ ,  $(20.8 \pm 1.6 \pm 2.3) \times 10^{-5}$ ;  $\mathcal{B}(\chi_{c0,1,2} \rightarrow \Sigma^0\bar{\Sigma}^0) = (47.8 \pm 3.4 \pm 3.9) \times 10^{-5}$ ,  $(3.8 \pm 1.0 \pm 0.5) \times 10^{-5}$ ,  $(4.0 \pm 1.1 \pm 0.5) \times 10^{-5}$ ; and  $\mathcal{B}(\chi_{c0,1,2} \rightarrow \Sigma^+\bar{\Sigma}^-) = (45.4 \pm 4.2 \pm 3.0) \times 10^{-5}$ ,  $(5.4 \pm 1.5 \pm 0.5) \times 10^{-5}$ ,  $(4.9 \pm 1.9 \pm 0.7) \times 10^{-5}$ , where the first error is statistical and the second is systematic. Upper limits on the branching fractions for the decays of  $\chi_{c1,2} \rightarrow \Sigma^0\bar{\Sigma}^0$ ,  $\Sigma^+\bar{\Sigma}^-$  are estimated to be  $\mathcal{B}(\chi_{c1} \rightarrow \Sigma^0\bar{\Sigma}^0) < 6.2 \times 10^{-5}$ ,  $\mathcal{B}(\chi_{c2} \rightarrow \Sigma^0\bar{\Sigma}^0) < 6.5 \times 10^{-5}$ ,  $\mathcal{B}(\chi_{c1} \rightarrow \Sigma^+\bar{\Sigma}^-) < 8.7 \times 10^{-5}$  and  $\mathcal{B}(\chi_{c2} \rightarrow \Sigma^+\bar{\Sigma}^-) < 8.8 \times 10^{-5}$  at the 90% confidence level.

DOI: [10.1103/PhysRevD.87.032007](https://doi.org/10.1103/PhysRevD.87.032007)

PACS numbers: 12.38.Qk, 13.25.Gv, 14.20.Gk

\* Also at the Moscow Institute of Physics Technology, Moscow 141700, Russia.

† On leave from the Bogolyubov Institute for Theoretical Physics, Kiev 03680, Ukraine.

‡ Also at the PNPI, Gatchina 188300, Russia.

§ Present address: Nagoya University, Nagoya 464-8601, Japan.

## I. INTRODUCTION

In the standard quark model,  $\chi_{cJ}$  ( $J = 0, 1, 2$ ) mesons are  $c\bar{c}$  states in an  $L = 1$  configuration. Experimental studies on  $\chi_{cJ}$  decay properties are essential to test perturbative quantum chromodynamics (QCD) models and

QCD-based calculations. The importance of the color octet mechanism (COM) for  $\chi_{cJ}$  decays has been pointed out for many years [1], and theoretical predictions of two-body exclusive decays have been made based on it. The predictions of COM theory for some  $\chi_{cJ}$  decays into baryon pairs ( $B\bar{B}$ ) disagree with measured values. For example, the branching fraction of  $\chi_{c0} \rightarrow \Lambda\bar{\Lambda}$  is predicted to be  $(93.5 \pm 20.5) \times 10^{-5}$  according to Ref. [2] and  $(11.9\text{--}15.1) \times 10^{-5}$  according to Ref. [3], while the world average of experimental measurements is  $(33.0 \pm 4.0) \times 10^{-5}$  [4]. One finds that the theoretical prediction is either about 2 times larger or several times smaller than the experimental measurement. Although some experimental results on  $\chi_{cJ}$  exclusive decays have been reported [5–7], many decay modes of  $\chi_{cJ} \rightarrow B\bar{B}$  have not been observed yet, such as  $\chi_{c1,2} \rightarrow \Sigma^0\bar{\Sigma}^0$ ,  $\Sigma^+\bar{\Sigma}^-$ , or measured with poor precision. For further testing of the COM in the decays of the  $P$ -wave charmonia, measurements of other baryon pair decays of  $\chi_{cJ}$ , such as  $\chi_{cJ} \rightarrow \Lambda\bar{\Lambda}$ ,  $\Sigma^0\bar{\Sigma}^0$  and  $\Sigma^+\bar{\Sigma}^-$ , are desired.

In addition, measurements of  $\chi_{c0} \rightarrow B\bar{B}$  are helpful for further understanding the helicity selection rule [8], which prohibits  $\chi_{c0}$  decays into baryon-antibaryon pairs. However, the measured branching fractions for  $\chi_{c0} \rightarrow B\bar{B}$  do not vanish, for example,  $\chi_{c0} \rightarrow p\bar{p}$  [4], which demonstrates a strong violation of the helicity selection rule in charmonium decays. It is necessary to measure the decays of  $\chi_{c0} \rightarrow B\bar{B}$  in other channels to provide additional tests of the helicity selection rule.

While  $\chi_{cJ}$  mesons are not produced directly in  $e^+e^-$  annihilations, the large branching fractions of  $\psi' \rightarrow \gamma\chi_{cJ}$  make  $e^+e^-$  collision at the  $\psi'$  peak a very clean environment for  $\chi_{cJ}$  investigation. In this paper, the results of two-body decays of  $\chi_{cJ} \rightarrow \Lambda\bar{\Lambda}$ ,  $\Sigma^0\bar{\Sigma}^0$  and  $\Sigma^+\bar{\Sigma}^-$  final states are presented. This analysis is based on  $106 \times 10^6$   $\psi'$  events [9] collected with BESIII at the BEPCII. A sample of  $44 \text{ pb}^{-1}$  of data taken at  $\sqrt{s} = 3.65 \text{ GeV}$  is used for continuum background study.

## II. BESIII DETECTOR AND MONTE CARLO SIMULATION

BEPCII is a double-ring  $e^+e^-$  collider that has reached peak luminosity of about  $0.6 \times 10^{33} \text{ cm}^{-2} \text{ s}^{-1}$  at the peak energy of  $\psi(3770)$ . The cylindrical core of the BESIII detector consists of a helium-based main drift chamber (MDC), a plastic scintillator time-of-flight system, and a CsI(Tl) electromagnetic calorimeter (EMC), which are all enclosed in a superconducting solenoidal magnet providing a 1.0 T magnetic field. The solenoid is supported by an octagonal flux-return yoke with resistive plate counter muon identifier modules interleaved with steel. The acceptance for charged particles and photons is 93% over  $4\pi$  stereo angle, and the charged-particle momentum and photon energy resolutions at 1 GeV are 0.5% and 2.5%, respectively. The detector is described in more detail in Ref. [10].

The BESIII detector is modeled with a Monte Carlo (MC) simulation based on GEANT4 [11,12]. The  $\psi'$  resonance is produced with KKMC [13], while the subsequent decays are generated with EVTGEN [14] according to the branching fractions provided by the particle data group (PDG) [4], and the remaining unmeasured decay modes are generated with LUNDCHARM [15].

## III. EVENT SELECTION

The investigated final states include  $\Lambda(\bar{\Lambda})$ ,  $p(\bar{p})$ , neutral  $\pi^0$  mesons and a radiative photon from the decay  $\psi' \rightarrow \gamma\chi_{cJ}$ , where  $\Lambda(\bar{\Lambda})$  decays to  $\pi^-p$  ( $\pi^+\bar{p}$ ), while  $\pi^0$  is reconstructed in the decay to  $\pi^0 \rightarrow \gamma\gamma$ . Candidate events are required to satisfy the following selection criteria. A charged track should have good quality in the track fitting and be within the angle coverage of the MDC ( $|\cos\theta| < 0.92$ ). Photons are reconstructed from isolated showers in the EMC. The energy deposited in the nearby time-of-flight counter is included to improve the reconstruction efficiency and energy resolution. Photon energies are required to be greater than 25 MeV in the EMC barrel region ( $|\cos\theta| < 0.8$ ) and greater than 50 MeV in the EMC end cap ( $0.86 < |\cos\theta| < 0.92$ ). The showers in the angular range between the barrel and the end cap are poorly reconstructed and excluded from the analysis. Moreover, the EMC timing of the photon candidate must be in coincidence with collision events,  $0 \leq t \leq 700 \text{ ns}$ , to suppress electronic noise and energy deposits unrelated to the events.

### A. $\chi_{cJ} \rightarrow \Lambda\bar{\Lambda}$

Candidate events contain at least two positively charged tracks, two negatively charged tracks and one photon. The  $\Lambda(\bar{\Lambda})$  candidates are reconstructed from pairs of oppositely charged tracks, which are constrained to secondary vertices and have invariant masses closest to the nominal  $\Lambda$  mass. The  $\chi^2$  of the secondary vertex fit must be less than 500. The candidate photon and the  $\Lambda\bar{\Lambda}$  pair are subjected to a four constraint (4C) kinematic fit under the hypothesis of  $\psi' \rightarrow \gamma\Lambda\bar{\Lambda}$  to reduce background and improve the mass resolution. When additional photons are found in an event, all possible combinations are iterated over, and the one with the best kinematic fit  $\chi^2_{4C}$  is kept. Furthermore,  $\chi^2_{4C} < 50$  is required to suppress potential background from  $\psi' \rightarrow \Sigma^0\bar{\Sigma}^0$ . The  $\chi^2_{4C}$  selection criterion is determined by optimizing the figure of merit (FOM),  $\text{FOM} = \frac{S}{\sqrt{S+B}}$ , where  $S$  is the number of signal events and  $B$  is the number of background events based on the MC simulation. Figure 1(a) shows the comparison of  $\chi^2_{4C}$  between data and MC simulation, which is normalized with the number of events satisfying the  $\chi^2$  requirement. Figure 1(b) shows the scatter plots of  $M_{p\pi^-}$  versus  $M_{\bar{p}\pi^+}$  from the data. Clear  $\Lambda\bar{\Lambda}$  signals can be seen. The square around the  $\Lambda$  nominal mass with a width of  $20 \text{ MeV}/c^2$  is taken as the signal

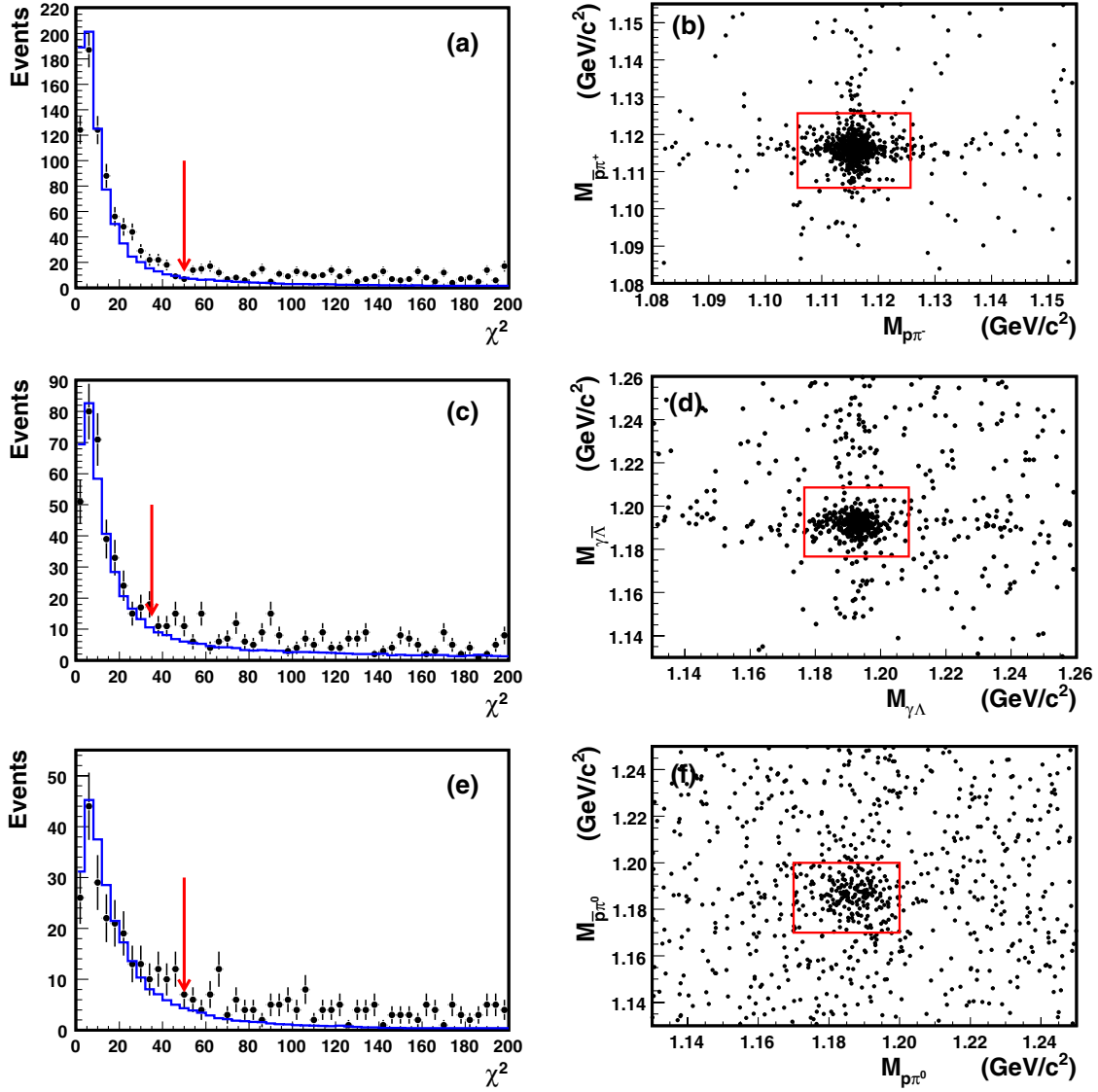


FIG. 1 (color online). (a) The  $\chi_{4C}^2$  distribution and (b)  $M_{p\pi^-}$  versus  $M_{\bar{p}\pi^+}$  (data) for the  $\psi' \rightarrow \gamma\chi_{cJ}, \chi_{cJ} \rightarrow \Lambda\bar{\Lambda}$  candidates; (c) the  $\chi_{4C}^2$  distribution and (d)  $M_{\gamma\Lambda}$  versus  $M_{\gamma\bar{\Lambda}}$  (data) for the  $\psi' \rightarrow \gamma\chi_{cJ}, \chi_{cJ} \rightarrow \Sigma^0\bar{\Sigma}^0$  candidates; (e) the  $\chi_{4C}^2$  distribution and (f)  $M_{p\pi^0}$  versus  $M_{\bar{p}\pi^0}$  (data) for the  $\psi' \rightarrow \gamma\chi_{cJ}, \chi_{cJ} \rightarrow \Sigma^+\bar{\Sigma}^-$  candidates.

region, which is also determined by maximizing the FOM. From events with two or more photons, additional selection criteria are applied to suppress backgrounds from  $\Sigma^0\bar{\Sigma}^0$  decays. The  $\psi' \rightarrow \Sigma^0\bar{\Sigma}^0$  candidates are selected by minimizing  $\sqrt{(M_{\gamma\Lambda} - M_{\Sigma^0})^2 + (M_{\gamma\bar{\Lambda}} - M_{\bar{\Sigma}^0})^2}$  from all combinations. However, some backgrounds remain in the signal region from  $\psi' \rightarrow \Sigma^0\bar{\Sigma}^0$  events in which one photon from the  $\Sigma^0$  decays is not reconstructed. To remove these, events falling into  $|M_{\gamma\Lambda} - M_{\Sigma^0}| < 6 \text{ MeV}/c^2$  and  $|M_{\gamma\bar{\Lambda}} - M_{\bar{\Sigma}^0}| < 6 \text{ MeV}/c^2$  have been discarded.

### B. $\chi_{cJ} \rightarrow \Sigma^0\bar{\Sigma}^0$

Candidate events have at least two positively charged tracks, two negatively charged tracks and three photons.

The charged track selection and  $\Lambda(\bar{\Lambda})$  reconstruction are the same as described above for the  $\chi_{cJ} \rightarrow \Lambda\bar{\Lambda}$  decay. The mass window of  $\Lambda(\bar{\Lambda})$  is optimized to be  $|M_{p\pi} - M_{\Lambda}| < 7 \text{ MeV}/c^2$ . The candidate photons and the  $\Lambda\bar{\Lambda}$  pair are subjected to a 4C kinematic fit under the hypothesis of  $\psi' \rightarrow \gamma\gamma\gamma\Lambda\bar{\Lambda}$  to reduce background and improve the mass resolution. When additional photons are found in an event, all possible combinations are looped over, the one with the smallest  $\chi_{4C}^2$  is kept, and  $\chi_{4C}^2 < 35$  is required to suppress the dominant background from  $\psi' \rightarrow \Sigma^0\bar{\Sigma}^0$ . Figure 1(c) shows the comparison of  $\chi_{4C}^2$  between data and MC simulation, which is normalized with the number of events satisfying the  $\chi^2$  requirement. The  $\Sigma^0\bar{\Sigma}^0$  candidates are chosen by

minimizing  $\sqrt{(M_{\gamma\Lambda} - M_{\Sigma^0})^2 + (M_{\gamma\bar{\Lambda}} - M_{\bar{\Sigma}^0})^2}$ . Figure 1(d) shows the scatter plot of  $M_{\gamma\Lambda}$  versus  $M_{\gamma\bar{\Lambda}}$  from the data. Clear  $\Sigma^0\bar{\Sigma}^0$  signals can be seen. The square around the  $\Sigma^0$  nominal mass with a width of  $32 \text{ MeV}/c^2$  represents the signal region.

### C. $\chi_{cJ} \rightarrow \Sigma^+ \bar{\Sigma}^-$

Candidate events contain at least one positively charged, one negatively charged tracks and five photons. We impose a 4C kinematic fit to the selected tracks and photons under the  $\psi' \rightarrow 5\gamma p \bar{p}$  hypothesis and keep the one with the smallest  $\chi_{4C}^2$ , and  $\chi_{4C}^2 < 50$  is required to suppress the dominant background from  $\psi' \rightarrow \Sigma^+ \bar{\Sigma}^-$ . Figure 1(e) shows the comparison of  $\chi_{4C}^2$  between data and MC simulation, which is normalized with the number of events satisfying the  $\chi^2$  requirement. The  $\pi^0$  candidates are reconstructed by selecting the combination which minimizes  $\sqrt{(M_{\gamma\gamma}^{(1)} - M_{\pi^0})^2 + (M_{\gamma\gamma}^{(2)} - M_{\pi^0})^2}$ . The  $\Sigma^+ \bar{\Sigma}^-$  pair is selected by minimizing  $\sqrt{(M_{p\pi^0} - M_{\Sigma^+})^2 + (M_{\bar{p}\pi^0} - M_{\bar{\Sigma}^-})^2}$ . Figure 1(f) shows the scatter plot of  $M_{p\pi^0}$  versus  $M_{\bar{p}\pi^0}$  from the data. Clear  $\Sigma^+ \bar{\Sigma}^-$  signals can be seen. The square of  $1.17 \text{ GeV}/c^2 < M_{p\pi^0} < 1.20 \text{ GeV}/c^2$  and  $1.17 \text{ GeV}/c^2 < M_{\bar{p}\pi^0} < 1.20 \text{ GeV}/c^2$  denotes the signal region.

## IV. BACKGROUND STUDY

### A. Continuum backgrounds

The events collected at  $E_{\text{cm}} = 3.65 \text{ GeV}$ , whose integrated luminosity is more than 1/4 of  $\psi'$  samples, are analyzed to estimate the contribution from the continuum process. No events are survived in the  $\Lambda\bar{\Lambda}$ ,  $\Sigma^0\bar{\Sigma}^0$  and  $\Sigma^+\bar{\Sigma}^-$  signal regions. Therefore, backgrounds from the continuum are neglected.

### B. Dominant backgrounds in $\Lambda\bar{\Lambda}$ , $\Sigma^0\bar{\Sigma}^0$ and $\Sigma^+\bar{\Sigma}^-$ final states

By using  $106 \times 10^6$  inclusive MC events, we find that the dominant background for  $\chi_{cJ} \rightarrow \Lambda\bar{\Lambda}$  comes from the decay  $\psi' \rightarrow \Sigma^0\bar{\Sigma}^0$  in which one photon is missing. The non- $\Lambda\bar{\Lambda}$  background from the decay  $\chi_{cJ} \rightarrow \pi^+ \pi^- p \bar{p}$  is negligibly small due to the low efficiency near the mass threshold. For  $\chi_{cJ} \rightarrow \Sigma^0\bar{\Sigma}^0$ , the dominant background is also found to arise from  $\psi' \rightarrow \Sigma^0\bar{\Sigma}^0$ . But this background mainly distributes around the  $\psi'$  mass region in the  $\Sigma^0\bar{\Sigma}^0$  invariant mass. In addition, a few background events come from  $\psi' \rightarrow \pi^0 \pi^0 J/\psi$  and  $\psi' \rightarrow \Xi^0 \bar{\Xi}^0$ . For  $\chi_{cJ} \rightarrow \Sigma^+ \bar{\Sigma}^-$ , the backgrounds are small; they are from the decay  $\psi' \rightarrow \Sigma^+ \bar{\Sigma}^-$ ,  $\psi' \rightarrow \pi^0 \pi^0 J/\psi$  and  $J/\psi \rightarrow p \bar{p}$  (or  $\gamma p \bar{p}$ ). The contributions of all backgrounds mentioned above are

estimated by MC simulation according to their branching fractions.

## V. FIT TO THE SIGNAL OF $\chi_{cJ}$

The invariant mass of the baryon pairs  $M_{B\bar{B}}$  for all selected events are shown in Figs. 2(a)–2(c) for  $\chi_{cJ} \rightarrow \Lambda\bar{\Lambda}$ ,  $\Sigma^0\bar{\Sigma}^0$  and  $\Sigma^+\bar{\Sigma}^-$ , respectively. Clear  $\chi_{c0,1,2}$  signals can be seen in  $\Lambda\bar{\Lambda}$  final state, and a clear  $\chi_{c0}$  signal is seen in both  $\Sigma^0\bar{\Sigma}^0$  and  $\Sigma^+\bar{\Sigma}^-$  final states, while the  $\chi_{c1,2}$  signals are not significant in  $\Sigma^0\bar{\Sigma}^0$  and  $\Sigma^+\bar{\Sigma}^-$  final states. We fit the invariant mass spectra of baryon pairs,  $M_{B\bar{B}}$ , to extract the numbers of  $\chi_{cJ}$  signal events, where the signals are represented by Breit-Wigner functions convolved with a Crystal Ball function to account for the detector resolution, a second-order Chebychev polynomial is used to describe non-peaking backgrounds, and the dominant background events, estimated by MC simulation, have been directly subtracted from the data. The widths of the Breit-Wigner functions were fixed according to the known values [4], the parameters of the Crystal Ball function are fixed based on MC simulation, and these parameters are varied by  $\pm\sigma$  for the determination of systematic uncertainties. To determine the goodness of fit, we bin the data so that the number of events in each bin is at least ten. The calculated  $\chi^2/\text{d.o.f.}$  is 1.03, 1.53 and 1.71 for the  $\Lambda\bar{\Lambda}$ ,  $\Sigma^0\bar{\Sigma}^0$  and  $\Sigma^+\bar{\Sigma}^-$  final states, respectively. The numbers of  $\chi_{c0,1,2}$  signal events from the fits are listed in Table I. For the

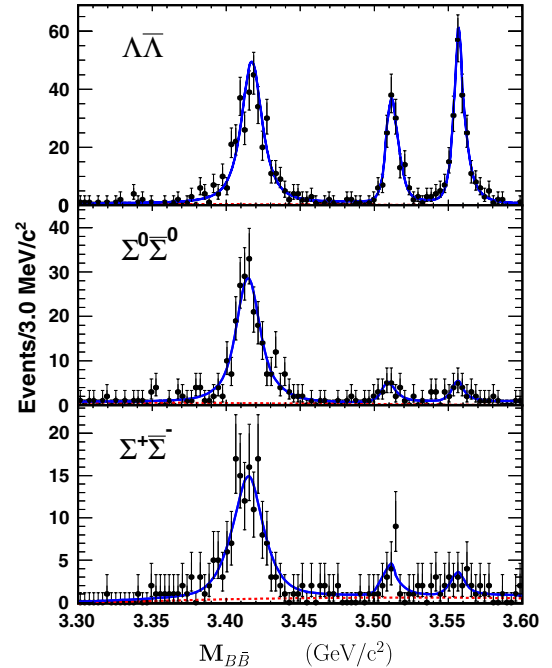


FIG. 2 (color online). The fit to the invariant mass  $M_{B\bar{B}}$ . Dots with error bars are for data. The solid line is the fit results. The dashed line is other background. The parameters of signal function are fixed to those obtained from MC simulation.

TABLE I. Efficiencies ( $\epsilon$  in %) obtained from MC simulation, and the signal yields  $N^{\text{obs}}$  determined from fit.

Mode	$\chi_{c0}$		$\chi_{c1}$		$\chi_{c2}$	
	$N^{\text{obs}}$	$\epsilon$	$N^{\text{obs}}$	$\epsilon$	$N^{\text{obs}}$	$\epsilon$
$\Lambda\bar{\Lambda}$	$368.9 \pm 22.1$	$26.6 \pm 0.2$	$135.6 \pm 12.6$	$27.9 \pm 0.2$	$207.1 \pm 15.7$	$26.3 \pm 0.2$
$\Sigma^0\bar{\Sigma}^0$	$242.8 \pm 17.1$	$12.2 \pm 0.1$	$20.0 \pm 5.3$	$13.2 \pm 0.1$	$18.9 \pm 5.3$	$12.7 \pm 0.1$
$\Sigma^+\bar{\Sigma}^-$	$147.8 \pm 13.8$	$12.3 \pm 0.1$	$18.0 \pm 5.4$	$13.1 \pm 0.1$	$14.5 \pm 5.6$	$12.3 \pm 0.1$

decay  $\chi_{c1,2} \rightarrow \Sigma^0\bar{\Sigma}^0$ ,  $\Sigma^+\bar{\Sigma}^-$ , the upper limits of the branching fractions at the 90% C.L. are also determined with a Bayesian method [16]. The statistical significances of the signals are calculated as  $\sqrt{-2\Delta \ln \mathcal{L}}$ , where  $\Delta \ln \mathcal{L}$  is the difference between the logarithmic maximum likelihood values of the fit with and without the corresponding signal function. They are  $4.3\sigma$  and  $4.6\sigma$  for  $\chi_{c1,2} \rightarrow \Sigma^0\bar{\Sigma}^0$ , and  $4.4\sigma$  and  $3.0\sigma$  for  $\chi_{c1,2} \rightarrow \Sigma^+\bar{\Sigma}^-$ , respectively. The signal efficiencies determined from MC simulation are also listed in Table I, where the proper angular distributions for photons emitted in  $\psi' \rightarrow \gamma\chi_{cJ}$  are used [17]. The decay of  $\chi_{cJ} \rightarrow B\bar{B}$  and the decay of baryons are generated with a phase space model.

## VI. SYSTEMATIC ERROR

The systematic errors mainly originate from the uncertainties of the tracking efficiency,  $\Lambda(\bar{\Lambda})$  reconstruction efficiency, the photon efficiency, 4C kinematic fit, the branching fractions of the intermediate states, fit range, the angular distribution of  $\chi_{c1,2} \rightarrow B\bar{B}$ , background shape, signal line shape, MC resolution and the total number of  $\psi'$  events.

- (1) The decay  $\psi' \rightarrow \Lambda\bar{\Lambda}$  with  $\Lambda \rightarrow p\pi^-$  and  $\Lambda \rightarrow \bar{p}\pi^+$  is employed to study the  $\Lambda(\bar{\Lambda})$  reconstruction efficiency. The selection criteria of charged tracks are the same as before except we use particle identification information to suppress background. Candidate events have at least one positively charged and one negatively charged track, which are required to be identified as a  $\pi^+(\pi^-)$  track and an  $\bar{p}(p)$  track, respectively. Also, the invariant mass of  $\pi^+\bar{p}(\pi^-\bar{p})$  must be within 10 MeV/ $c^2$  of the nominal  $\bar{\Lambda}$  mass. Furthermore, the momentum of  $\bar{\Lambda}(\Lambda)$  candidates is required to be within 20 MeV/ $c$  of its nominal value in two-body decay of  $\psi' \rightarrow \Lambda\bar{\Lambda}$ . The number of  $\Lambda$  signal events,  $N_{\Lambda}^0$ , is extracted by fitting the recoiling mass spectrum of  $\bar{\Lambda}$ ,  $M_{\text{recoil}}^{\bar{\Lambda}}$ . Then two additional oppositive charged tracks, a  $\pi^-(\pi^+)$  and a  $p(\bar{p})$ , are required to reconstruct  $\Lambda$  and are constrained to the secondary vertex. The number of  $\Lambda$  signal events,  $N_{\Lambda}^1$ , is extracted by fitting  $M_{\text{recoil}}^{\bar{\Lambda}}$  after requiring a  $\Lambda$  secondary vertex constraint. The  $\Lambda(\bar{\Lambda})$  reconstruction efficiency is

determined as  $\epsilon_{\Lambda} = \frac{N_{\Lambda}^1}{N_{\Lambda}^0}$ . The difference of the efficiencies between data and MC simulation is found to be 2.0% for a  $\Lambda$  and 5.0% for a  $\bar{\Lambda}$ , which are taken as the systematic error due to  $\Lambda(\bar{\Lambda})$  reconstruction efficiency.

- (2) Since the decay length for  $\Sigma^+(\bar{\Sigma}^-)$  is small, the decay  $J/\psi \rightarrow \pi^+\pi^-p\bar{p}$  is used to study the MDC tracking efficiency for the proton and antiproton of the  $\Sigma^+\bar{\Sigma}^-$  final state. It is found that the efficiency for MC simulated events agrees with that determined from data within 1.0% for each charged track. Hence, 2.0% is taken as the systematic error for the proton and antiproton of the  $\Sigma^+\bar{\Sigma}^-$  final state.
- (3) The uncertainty due to photon detection efficiency is 1% per photon, which is determined from the decay  $J/\psi \rightarrow \rho\pi$  [18].
- (4) Five decays,  $J/\psi \rightarrow \Lambda\bar{\Lambda}$ ,  $J/\psi \rightarrow \Sigma^0\bar{\Sigma}^0$ ,  $J/\psi \rightarrow \Xi^0\bar{\Xi}^0$ ,  $\psi' \rightarrow \pi^0\pi^0J/\psi$  ( $J/\psi \rightarrow p\bar{p}$ ) and  $\psi' \rightarrow \pi^0\pi^0J/\psi$  ( $J/\psi \rightarrow p\bar{p}\pi^0$ ), are used to study the efficiencies of the 4C kinematic fits. The signal events are selected from data and inclusive MC events without the 4C fit information. The remaining background is found to be negligible according to the studies of the inclusive MC events. The efficiency of the 4C kinematic fit is defined as  $\frac{N_1}{N_0}$ , where  $N_0$  is the the number of signal events and  $N_1$  is the number of events survived. For the  $\chi_{cJ} \rightarrow \Lambda\bar{\Lambda}$ , where the final state is  $\psi' \rightarrow \gamma\Lambda\bar{\Lambda}$ , two decays,  $J/\psi \rightarrow \Lambda\bar{\Lambda}$ , and  $J/\psi \rightarrow \Sigma^0\bar{\Sigma}^0$ , are used to investigate the systematic error due to the 4C kinematic fit. The final states of these two control samples contain one photon less or more than the signal channel. Conservatively, the larger difference observed in the two control samples, 2.4%, is taken as the systematic error. Similarly, the larger difference in  $J/\psi \rightarrow \Sigma^0\bar{\Sigma}^0$  and  $J/\psi \rightarrow \Xi^0\bar{\Xi}^0$ , 2.9%, is taken as the systematic error of the  $\chi_{cJ} \rightarrow \Sigma^0\bar{\Sigma}^0$  channel, and the larger difference in  $\psi' \rightarrow \pi^0\pi^0J/\psi$  ( $J/\psi \rightarrow p\bar{p}$ ) and  $\psi' \rightarrow \pi^0\pi^0J/\psi$  ( $J/\psi \rightarrow p\bar{p}\pi^0$ ), 1.3%, is taken as the error of  $\chi_{cJ} \rightarrow \Sigma^+\bar{\Sigma}^-$ .
- (5) When changing mass ranges in fitting  $M_{B\bar{B}}$  signals to 3.30–3.62 GeV/ $c^2$  or to 3.25–3.62 GeV/ $c^2$ , the fitted numbers of  $\chi_{c0,1,2}$  have some changes for data

and MC simulation. Taking the  $\Lambda\bar{\Lambda}$  channel as an example, the results in the range of 3.30–3.60 GeV/ $c^2$  are taken as central values, when the fit range is changed to 3.32–3.60 GeV/ $c^2$ , the changes relative to central values are found to be 2.7%, 3.6% and 2.2% for the  $\chi_{c0,1,2}$  decays, respectively, while in the range 3.25–3.62 GeV/ $c^2$ , the changes are found to be 2.2%, 0.9%, and 4.3%. Conservatively, we take the larger ones, 2.7%, 3.6% and 4.3%, as the systematic errors for the  $\Lambda\bar{\Lambda}$  final state. With the same method, the systematic errors for the other two channels are determined to be 1.4%, 6.7%, and 4.3% for the  $\Sigma^0\bar{\Sigma}^0$  final state and 1.4%, 3.0%, and 7.2% for the  $\Sigma^+\bar{\Sigma}^-$  final state.

- (6) In the fits to the  $M_{B\bar{B}}$  invariant mass, the signals are described by a parameterized shape obtained from MC simulation in which the widths of  $\chi_{cJ}$  are fixed since we only observe a small number of signal events in  $\chi_{c1,2} \rightarrow \Sigma^0\bar{\Sigma}^0$  and  $\Sigma^+\bar{\Sigma}^-$ . When changing the parameters of  $\chi_{cJ}$  widths in this MC simulation by  $\pm\sigma$ , it is found that the difference of the numbers of fitted  $\chi_{c1,2}$  events between data and MC is 1.2%, 0.0%, and 0.0% for the  $\Lambda\bar{\Lambda}$  final state; 1.9%, 0.0%, and 3.7% for the  $\Sigma^0\bar{\Sigma}^0$  final state; and 1.0%, 0.5%, and 2.0% for the  $\Sigma^+\bar{\Sigma}^-$  final state. Hence, we take the difference as the systematic error due to the  $\chi_{cJ}$  widths.
- (7) The partial width for an  $E1/M1$  radiative transition is proportional to the cube of the radiative photon energy ( $E_\gamma^3$ ), which leads to a diverging tail in the lower mass region. Two damping factors have been

proposed by the KEDR [19] and the CLEO [20] Collaborations and have been included to describe the signal line shape. Differences in the signal yields with respect to the fit not taking into account this damping factor are observed, and the greater differences are 0.7%, 2.1%, and 2.7% for the  $\Lambda\bar{\Lambda}$  final state; 1.4%, 1.0%, and 2.2% for the  $\Sigma^0\bar{\Sigma}^0$  final state; and 0.0%, 2.7%, and 5.5% for the  $\Sigma^+\bar{\Sigma}^-$  final state, which are taken as the systematic error associated with the signal line shape.

- (8) From the decay  $J/\psi \rightarrow \Lambda\bar{\Lambda}$ , it is found that the average resolution is  $7.90 \pm 0.09$  MeV/ $c^2$  for the data and  $7.08 \pm 0.04$  MeV/ $c^2$  for MC. Differences in fitting the  $\chi_{cJ}$  signal with and without fixing the MC parameters are found to be 1.5%, 0.5% and 2.4% for the  $\Lambda\bar{\Lambda}$  final states, which are taken as the systematic error of the resolution. However, from the decays  $J/\psi \rightarrow \Sigma^0\bar{\Sigma}^0$  and  $J/\psi \rightarrow \Sigma^+\bar{\Sigma}^-$ , one can find that the resolutions between data and MC are consistent. Therefore, the systematic errors of the resolution for the  $\Sigma^0\bar{\Sigma}^0$  and  $\Sigma^+\bar{\Sigma}^-$  final state are neglected.
- (9) To estimate the uncertainty of the angular distribution, we use another model in which the angular distribution of  $\chi_{c1,2} \rightarrow B\bar{B}$  is taken into account according to the helicity amplitude [21]. When the two independent helicity amplitudes,  $B_{\frac{1}{2}-\frac{1}{2}}$  and  $B_{-\frac{1}{2}\frac{1}{2}}$ , are set to be 1.0, the efficiencies are found to be  $(28.8 \pm 0.2)\%$  and  $(27.9 \pm 0.2)\%$  for the  $\chi_{c1,2} \rightarrow \Lambda\bar{\Lambda}$  final state, respectively. The differences from phase space are 3.2% and 6.0%. Similar comparisons are also done for the  $\Sigma^0\bar{\Sigma}^0$

TABLE II. Systematic errors in the branching fraction measurements (%).

Source	$\chi_{cJ} \rightarrow \Lambda\bar{\Lambda}$			$\chi_{cJ} \rightarrow \Sigma^0\bar{\Sigma}^0$			$\chi_{cJ} \rightarrow \Sigma^+\bar{\Sigma}^-$		
	$\chi_{c0}$	$\chi_{c1}$	$\chi_{c2}$	$\chi_{c0}$	$\chi_{c1}$	$\chi_{c2}$	$\chi_{c0}$	$\chi_{c1}$	$\chi_{c2}$
The total number of $\psi'$	0.81	0.81	0.81	0.81	0.81	0.81	0.81	0.81	0.81
MDC tracking ( $p, \bar{p}$ )	...	...	...	...	...	...	2.0	2.0	2.0
Photon efficiency	1.0	1.0	1.0	3.0	3.0	3.0	5.0	5.0	5.0
$\Lambda$ reconstruction	2.0	2.0	2.0	2.0	2.0	2.0	...	...	...
$\bar{\Lambda}$ reconstruction	5.0	5.0	5.0	5.0	5.0	5.0	...	...	...
Kinematic fit	2.4	2.4	2.4	2.9	2.9	2.9	1.3	1.3	1.3
Fitting range	2.7	3.6	4.3	1.4	6.7	4.3	1.4	3.0	7.2
$\chi_{cJ}$ width	1.2	0.0	0.0	1.9	0.0	3.7	1.0	0.5	2.0
Angular distribution	0.0	3.2	6.0	0.0	3.2	6.0	0.0	3.2	6.0
Background shape	0.5	1.3	1.3	1.7	7.8	6.0	1.8	2.5	3.0
Signal line shape	0.7	2.1	2.7	1.4	1.0	2.2	0.0	2.7	5.5
MC resolution	1.5	0.5	2.4	0.0	0.0	0.0	0.0	0.0	0.0
$\mathcal{B}(\psi' \rightarrow \gamma\chi_{cJ})$	3.2	4.3	4.0	3.2	4.3	4.0	3.2	4.3	4.0
$\mathcal{B}(\Sigma \rightarrow p\pi)$	...	...	...	...	...	...	0.82	0.82	0.82
$\mathcal{B}(\Lambda \rightarrow p\pi)$	1.1	1.1	1.1	1.1	1.1	1.1	...	...	...
Total systematic error	7.7	9.3	11.1	8.3	13.6	13.2	7.0	9.1	13.4

TABLE III. Branching fractions (or their upper limits) of  $\chi_{cJ} \rightarrow \Lambda \bar{\Lambda}$ ,  $\Sigma^0 \bar{\Sigma}^0$  and  $\Sigma^+ \bar{\Sigma}^-$  (in units of  $10^{-5}$ ). The first error is statistical and the second is systematic.

Mode		$\chi_{c0}$	$\chi_{c1}$	$\chi_{c2}$
$\Lambda \bar{\Lambda}$	This work	$33.3 \pm 2.0 \pm 2.6$	$12.2 \pm 1.1 \pm 1.1$	$20.8 \pm 1.6 \pm 2.3$
	PDG	$33.0 \pm 4.0$	$11.8 \pm 1.9$	$18.6 \pm 2.7$
	CLEO	$33.8 \pm 3.6 \pm 2.2 \pm 1.7$	$11.6 \pm 1.8 \pm 0.7 \pm 0.7$	$17.0 \pm 2.2 \pm 1.1 \pm 1.1$
	Theory	$(93.5 \pm 20.5^a, 22.1 \pm 6.1^b)$ [2]	...	$(15.2 \pm 1.7^a, 4.3 \pm 0.6^b)$ [2]
$\Sigma^0 \bar{\Sigma}^0$		11.9–15.1 [3]	3.9 [22]	3.5 [22]
	This work	$47.8 \pm 3.4 \pm 3.9$	$3.8 \pm 1.0 \pm 0.5(<6.2)$	$4.0 \pm 1.1 \pm 0.5(<6.5)$
	PDG	$42.0 \pm 7.0$	$<4.0$	$<8.0$
	CLEO	$44.1 \pm 5.6 \pm 4.2 \pm 2.2$	$<4.4$	$<7.5$
$\Sigma^+ \bar{\Sigma}^-$	Theory	$(25.1 \pm 3.4^a, 18.7 \pm 4.5^b)$ [2]	...	$(38.9 \pm 8.8^a, 4.2 \pm 0.5^b)$ [2]
		...	3.3 [22]	5.0 [22]
	This work	$45.4 \pm 4.2 \pm 3.0$	$5.4 \pm 1.5 \pm 0.5(<8.7)$	$4.9 \pm 1.9 \pm 0.7(<8.8)$
	PDG	$31.0 \pm 7.0$	$<6.0$	$<7.0$
$\Sigma^+ \bar{\Sigma}^-$	CLEO	$32.5 \pm 5.7 \pm 4.0 \pm 1.7$	$<6.5$	$<6.7$
	Theory	5.5–6.9 [3]	3.3 [22]	5.0 [22]

and  $\Sigma^+ \bar{\Sigma}^-$  final states, and the differences are smaller. Conservatively, we take the difference of the  $\Lambda \bar{\Lambda}$  final state as the systematic error of the angular distribution for all  $B\bar{B}$  final states.

- (10) In Fig. 2, the combinatorial background curves are fitted with a second-order Chebychev polynomial. The background function is changed to first- and third-order polynomials, and the largest difference is taken as the systematic error due to the uncertainty in the description of the background shape.
- (11) The total number of  $\psi'$  events are obtained by studying inclusive hadronic  $\psi'$  decays with an uncertainty of 0.81% [9].

Table II lists all systematic error contributions, and the total systematic error is obtained by adding the individual contributions in quadrature.

## VII. RESULTS

The branching fraction of  $\chi_{cJ} \rightarrow B\bar{B}$  is determined by

$$\mathcal{B}(\chi_{cJ} \rightarrow B\bar{B}) = \frac{N_{\psi'}^{\text{obs}}[\chi_{cJ}]}{N_{\psi'} \cdot \epsilon \cdot \prod_i \mathcal{B}_i},$$

and if the signal is not significant, the corresponding upper limit of branching fraction is set with

$$\mathcal{B}(\chi_{cJ} \rightarrow B\bar{B}) < \frac{N_{\text{UL}}^{\text{obs}}[\chi_{cJ}]}{N_{\psi'} \cdot \epsilon \cdot \prod_i \mathcal{B}_i \cdot (1.0 - \sigma_{\text{sys}})},$$

where  $N^{\text{obs}}$  is the number of observed signal events and  $N_{\text{UL}}^{\text{obs}}$  is the upper limit of the number of events,  $\epsilon$  is the detection efficiency shown in Table I,  $\sigma_{\text{sys}}$  is the relative the systematic error,  $N_{\psi'}$  is the total number of  $\psi'$  events [9], and  $\prod_i \mathcal{B}_i$  is the product of the branching fractions taken from the world average [4] for the  $\psi' \rightarrow \gamma \chi_{cJ}$  and

the other decays that are involved. With the numbers listed in Table I and the branching fractions for the relevant baryon decays, the branching fractions or the upper limits at the 90% C.L. for  $\chi_{cJ}$  decays are determined, as listed in Table III.

## VIII. SUMMARY

Three  $\chi_{cJ}$  decays to the baryon pairs are observed, and their branching fractions are measured at BESIII, which are consistent with the world averages within the errors. For the decay of  $\chi_{cJ} \rightarrow \Lambda \bar{\Lambda}$ , the experimental results are still inconsistent with theoretical predictions [2,3,22], which are helpful to check the theoretical model of decays of  $\chi_{cJ} \rightarrow \Lambda \bar{\Lambda}$ . For the decays of  $\chi_{c1,2} \rightarrow \Sigma^0 \bar{\Sigma}^0$  and  $\Sigma^+ \bar{\Sigma}^-$ , the significances are improved relative to the previous measurements, but the comparisons of their branching fractions between experiments and theoretical predictions are inconclusive due to the limited experimental precision.

## ACKNOWLEDGMENTS

The BESIII Collaboration thanks the staff of BEPCII and the computing center for their hard efforts. This work is supported in part by the Ministry of Science and Technology of China under Contracts No. 2009CB825200 and No. 2009CB825206; National Natural Science Foundation of China (NSFC) under Contracts No. 10625524, No.10821063, No. 10825524, No. 10835001, No. 10935007, No. 10975143, No. 10975047, No. 10979008, No. 11125525, and No. 11275057; Joint Funds of the National Natural Science Foundation of China under Contracts No. 11079008, No. 11079027, and No. 11179007; the Chinese Academy of Sciences (CAS) Large-Scale Scientific Facility Program; CAS under Contracts No. KJCX2-YW-N29 and No. KJCX2-YW-N45; 100



Talents Program of CAS; Istituto Nazionale di Fisica Nucleare, Italy; Ministry of Development of Turkey under Contract No. DPT2006K-120470; U.S. Department of Energy under Contracts No. DE-FG02-04ER41291, No. DE-FG02-91ER40682, and No. DE-FG02-

94ER40823; U.S. National Science Foundation; University of Groningen (RuG) and the Helmholtzzentrum fuer Schwerionenforschung GmbH (GSI), Darmstadt; WCU Program of National Research Foundation of Korea under Contract No. R32-2008-000-10155-0.

- 
- [1] G. T. Bodwin, E. Braaten, and G. P. Lepage, *Phys. Rev. D* **51**, 1125 (1995).
- [2] R. G. Ping, B. S. Zou, and H. C. Chiang, *Eur. Phys. J. A* **23**, 129 (2005).
- [3] X. H. Liu and Q. Zhao, *J. Phys. G* **38**, 035007 (2011).
- [4] K. Nakamura *et al.* (Particle Data Group), *J. Phys. G* **37**, 075021 (2010).
- [5] J. Z. Bai *et al.* (BES Collaboration), *Phys. Rev. D* **67**, 112001 (2003).
- [6] M. Ablikim *et al.* (BES Collaboration), *Phys. Rev. D* **73**, 052006 (2006).
- [7] P. Naik *et al.* (CLEO Collaboration), *Phys. Rev. D* **78**, 031101 (2008).
- [8] S. J. Brodsky and G. P. Lepage, *Phys. Rev. D* **24**, 2848 (1981).
- [9] M. Ablikim *et al.* (BESIII Collaboration), [arXiv:1209.6199](https://arxiv.org/abs/1209.6199) [Chin. Phys. C (to be published)].
- [10] M. Ablikim *et al.* (BESIII Collaboration), *Nucl. Instrum. Methods Phys. Res., Sect. A* **614**, 345 (2010).
- [11] S. Agostinelli *et al.* (GEANT4 Collaboration), *Nucl. Instrum. Methods Phys. Res., Sect. A* **506**, 250 (2003).
- [12] J. Allison *et al.*, *IEEE Trans. Nucl. Sci.* **53**, 270 (2006).
- [13] S. Jadach, B. F. L. Ward, and Z. Was, *Comput. Phys. Commun.* **130**, 260 (2000); *Phys. Rev. D* **63**, 113009 (2001).
- [14] R. G. Ping, *Chinese Phys. C* **32**, 599 (2008).
- [15] J. C. Chen, G. S. Huang, X. R. Qi, D. H. Zhang, and Y. S. Zhu, *Phys. Rev. D* **62**, 034003 (2000).
- [16] Y. S. Zhu, *Chinese Phys. C* **32**, 363 (2008).
- [17] W. M. Tanenbaum *et al.*, *Phys. Rev. D* **17**, 1731 (1978); G. Karl, S. Meshkov, and J. L. Rosner, *Phys. Rev. D* **13**, 1203 (1976); M. Oreglia *et al.*, *Phys. Rev. D* **25**, 2259 (1982).
- [18] M. Ablikim *et al.* (BESIII Collaboration), *Phys. Rev. D* **83**, 112005 (2011).
- [19] V. M. Malyshev, *Int. J. Mod. Phys. Conf. Ser.* **02**, 188 (2011).
- [20] R. E. Mitchell *et al.* (CLEO Collaboration), *Phys. Rev. Lett.* **102**, 011801 (2009).
- [21] G. R. Liao, R. G. Ping, and Y. X. Yang, *Chin. Phys. Lett.* **26**, 051101 (2009).
- [22] S. M. H. Wong, *Eur. Phys. J. C* **14**, 643 (2000).